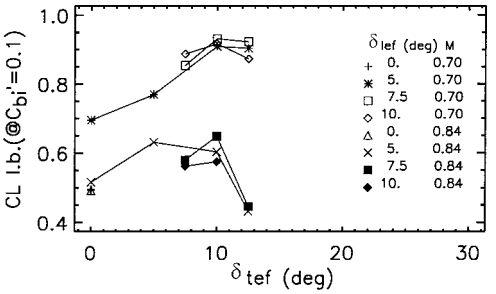

Fig. 4 $C_{\text{Ll.b.}}$ **vs** δ_{tef} **for different fixed** δ_{lef}**, at** $M = 0.70$ **and 0.84, based on** $C'_{\text{bi}} = 0.1$.

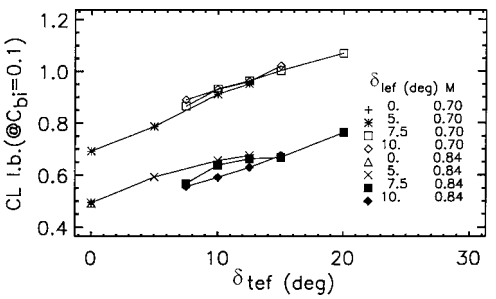

Fig. 5 Results for conditions described in Fig. 4 based on Proksch's light buffet criterion of $C_{\text{bi}} = 0.1$.

flap 7.5 deg downward and trailing-edge flap 10 deg downward. At $M = 0.84$, a 32% increment is achieved by the same flap deflection angles. The lift coefficient at light buffeting for the same flap configurations based on Proksch's C_{bi} method is shown in Fig. 5, showing an unrealistic phenomenon of ever-increasing $C_{\text{Ll.b.}}$ with increased deflection angle of the trailing-edge flap. Such a result contradicts empirical data for several other aircraft (see Refs. 7–10), whose light-buffet boundaries occur when δ_{tef} is much lower than 20 deg. Even in the absence of published test results for the ONERA M6 wing, we can conclude that the light buffet condition of $\delta_{\text{tef}} \sim 20$ deg for this wing is unrealistic, indicating that Proksch's method based on C_{bi} is not suitable for flapped wings.

Conclusions

For analyzing flapped-wing buffet behaviors, Proksch's buffet coefficient C_{bi}, commonly used for numerical prediction of buffet for wings without flap deflections, is modified and named C'_{bi} in this Note to take into account the volume of separated flow regions on the wing. The improvement in buffet analysis by using the modified buffet coefficient has been demonstrated in the numerical example of choosing proper flap scheduling for improving aircraft performance at transonic speeds. It shows that the proposed, modified buffet coefficient is possibly a more appropriate parameter for analyzing the buffet behavior of wings with strong flow separations.

References

[1]Proksch, H.-J., "Ermittlung der Buffeting-Grenzen von Kampfflugzeugen," Dornier GmbH Rept. EA 101/2916, 1973.

[2]Steger, J., Ying, S. X., and Schiff, L. B., "A Partially Flux Split Algorithm for Compressible Inviscid and Viscous Flow," *Proceedings of the Workshop Held by the Institute of Nonlinear Science at the University of California, Davis*, Inst. of Nonlinear Science, Univ. of California, La Jolla, CA, 1989.

[3]Baldwin, B. S., and Lomax, H., "Thin Layer Approximation and Algebraic Model for Separated Turbulent Flows," AIAA Paper 78-257, Jan. 1978.

[4]Schmitt, V., and Charpin, F., "Pressure Distributions on the ONERA M6 Wing at Transonic Mach Numbers," AGARD-AR-138, May 1979, pp. B1-1–B1-44.

[5]Ho, J.-Y., "Numerical Study of the Improvement on Transonic Wing Buffet by Flap Deflections," Ph.D. Dissertation, Univ. of Colorado, Boulder, CO, 1994.

[6]Thomas, F., and Redeker, G., "A Method for Calculating the Transonic Buffet Boundary Including the Influence of Reynolds Number," AGARD-CP-83, 1971.

[7]Ray, E. J., and Mickinney, L. W., "Maneuver and Buffet Characteristics of Fighter Aircraft," NASA-TN-D-7131, July 1973.

[8]Margolin, M., and Chung, J. G., "F-105F Transonic Buffet Study and Effect of Maneuvering Flaps," Air Force Flight Dynamics Lab., TR-69-37, July 1969.

[9]Friend, E. L., and Sefic, W. J., "Flight Measurement of Buffet Characteristics of the F-104 Airplane for Selected Wing-Flaps Deflections," NASA-TN-D-6943, Aug. 1972.

[10]Monaghan, R. C., and Friend, E. L., "Effects of Flaps on Buffet Characteristics and Wing-Rock Onset of an F-8C Airplane at Subsonic and Transonic Speeds," NASA-TM-X-2873, Aug. 1973.

Revisiting Unresolved Dynamic Stall Phenomena

Lars E. Ericsson*
Mountain View, California 94040

Introduction

THE rapid growth of the wind-turbine industry has generated renewed interest in the dynamic stall phenomenon due to the fact that wind-turbine blades operate continuously under stalled flow conditions.[1] In the literature search for Ref. 2, the present author ran across 30-year-old dynamic test results for a NACA-0012 airfoil section, oscillating around 25% chord[3] (Fig. 1), results that deviated dramatically from those expected[4] (Fig. 2). Although the two-dimensional test rig generated a highly three-dimensional flow separation pattern (Fig. 3), the lift measured by the balance at 25% chord should represent the general lift characteristics for two-dimensional unsteady airfoil stall. That is, the attached flow regions near the endplates at $\alpha = 12.3$ deg in Fig. 3a and at $\alpha = 14.6$ deg and 16.6 deg in Fig. 3b would have affected the magnitude of the measured $C_L(\alpha)$ but should not have distorted the general two-dimensional dynamic stall characteristics of the central wing area to make the lift measurements physically misleading. Consequently, the $C_L(\alpha)$ characteristics in Fig. 1 should have a two-dimensional phenomenological explanation. The carefully executed dynamic test, with its thoroughly documented experimental results, vividly illustrates how various flow phenomena could interact to distort the results obtained in subscale dynamic stall tests. The test results also describe full-scale flow interactions that could have significant influence on the unsteady aerodynamics of wind-turbine and helicopter blades.

Accelerated-Flow and Moving-Wall Effects

For the pitching airfoil in Fig. 1, the accelerated-flow effect and the Moving-wall effect act in unison.[5,6] Their combined effect can be represented by the dominating moving-wall effect, illustrated by classic Magnus lift results,[7] in both laminar (Fig. 4a) and turbulent (Fig. 4b) flow separation. The downstream moving-wall effect on the top side delays separation, and the upstream moving-wall effect on the bottom side promotes it. The combined effect is to generate a positive Magnus lift at $U_W / U_\infty < 0.3$ in Fig. 4a and at $U_W / U_\infty < 0.1$ in Fig. 4b. For the pitching airfoil, the corresponding moving-wall effect[6] is generated as shown in Fig. 5. During the upstroke (Fig. 5a), the flow velocity at the leading-edge surface has to be equal to the tangential surface velocity U_W to satisfy the no-slip condition. When the air flow has "rounded the corner" to the upper surface aft of the leading edge, U_W has decreased greatly,

Presented as Paper 2000-0144 at the 38th Aerospace Sciences Meeting, Reno, NV, 10–13 January 2000; received 19 March 2000; revision received 10 August 2000; accepted for publication 10 August 2000.

*Engineering Consultant. Fellow AIAA.

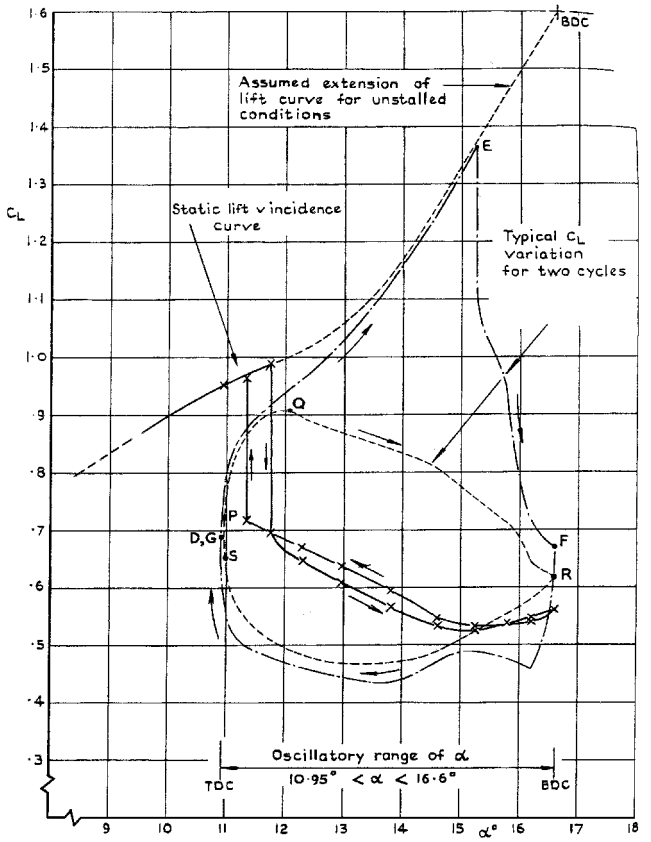

a) Transition fixed; $Re = 1.68 \times 10^6$, $\alpha_o = 13.78$ deg, $\Delta\theta = 2.83$ deg, and $\bar{\omega} = 0.117$

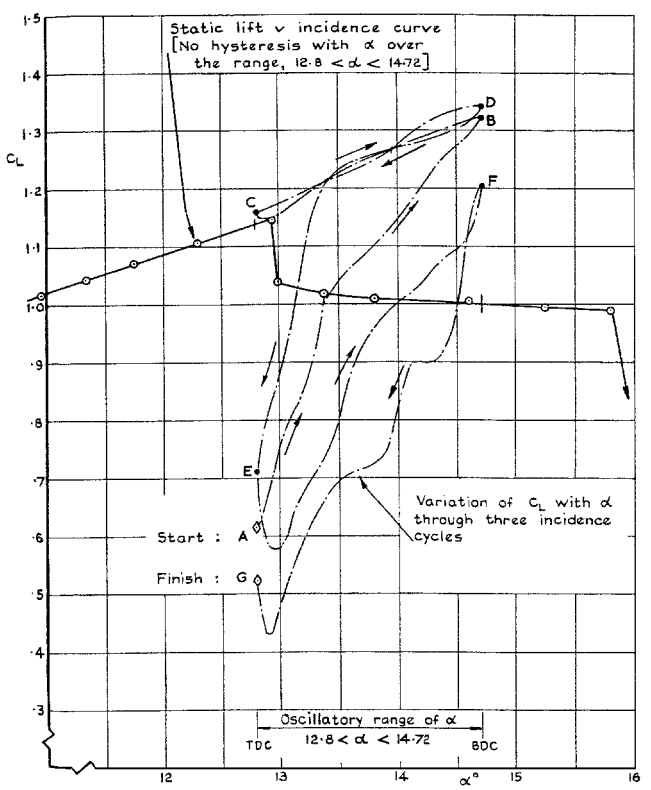

b) Transition free; $Re = 0.84 \times 10^6$, $\alpha_o = 13.76$ deg, $\Delta\theta = 1.92$ deg, and $\bar{\omega} = 0.369$

Fig. 1 $C_L(\alpha)$ characteristics of a NACA-0012 airfoil describing oscillations in pitch around 25% chord.[3]

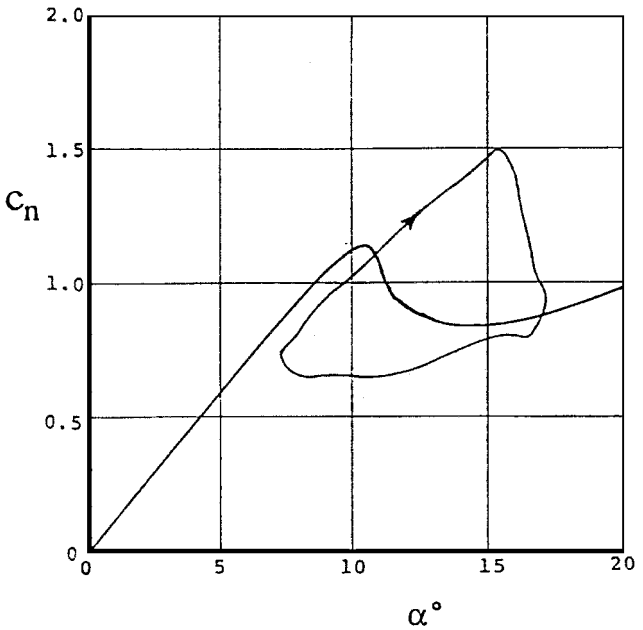

Fig. 2 $c_n(\alpha)$ characteristics of a NACA-0012 airfoil describing oscillations in pitch around 25% chord; $\alpha_o = 12.25$ deg, $\Delta\theta = 4.80$ deg, and $\bar{\omega} = 0.252$ (Ref. 4).

leaving the near-wall boundary layer with an excess velocity. This wall-motion-induced wall-jet effect improves the boundary layer profile,[6] thereby delaying the downstream flow separation. On the downstroke (Fig. 5b), the motion-induced wall-jet effect on the top side generates a separation-prone boundary-layer profile that promotes downstream flow separation. The effect can be visualized as the illustrated "roller" effect created by a rolling leading-edge cylinder of radius r_N.

Role Played by Boundary-Layer Transition

The moving-wall effect described by Figs. 4 and 5 explains the general data trend in Fig. 1a for "transition fixed" at $U_\infty = 200$ fps and $Re = 1.68 \times 10^6$. The peculiar $C_L(\alpha)$ branch D–E–F will be discussed later. Thus, the lift during the upstroke is larger than in the static test and is less than static during the downstroke. More consternating are the pitching loops recorded for "free transition" at $U_\infty = 100$ fps and $Re = 0.84 \times 10^6$ (Fig. 1b). The upstroke branch A–B generates less lift than the downstroke branches B–C and D–E. The following informative statement made in Ref. 3 regarding the static flow characteristics provides the clue: "With transition free, the transition position at the high incidences of these tests occurs at the reattachment point aft of the laminar separation bubble near the leading-edge on the wing upper surface. This bubble was, of course, very much more in evidence at the lower wind speed" (e.g., at $U_\infty = 100$ fps and $Re = 0.84 \times 10^6$ in Fig. 1b).

It is shown in Ref. 8 how the accelerated-flow and moving-wall effects on flow separation are reversed when they influence separation via their effects on boundary-layer transition. Against this background, the results in Fig. 1b can be explained as follows by the dominant moving-wall effects, again utilizing Magnus lift results[7] (Figs. 4 and 6) for illustration purposes. Figure 6 shows that the presence of the laminar separation bubble (curves j and k) can double the size of the Magnus lift reversal (curves d, e, and f). In the present test,[3] transition occurred shortly downstream of the laminar separation bubble. The adverse moving-wall effect generated during the pitch-down motion (Fig. 5b) apparently promoted transition to occur in the separation bubble. Applying the flow physics of the Magnus lift reversal in Fig. 6 to the airfoil top surface during the pitch-down motion (Fig. 5b), one expects the airfoil lift in Fig. 1b to be larger during the pitch-down branches B–C and D–E than during the pitch-up branch A–B, all in agreement with the experimental results.[3] However, it still remains to explain why the upstroke branch

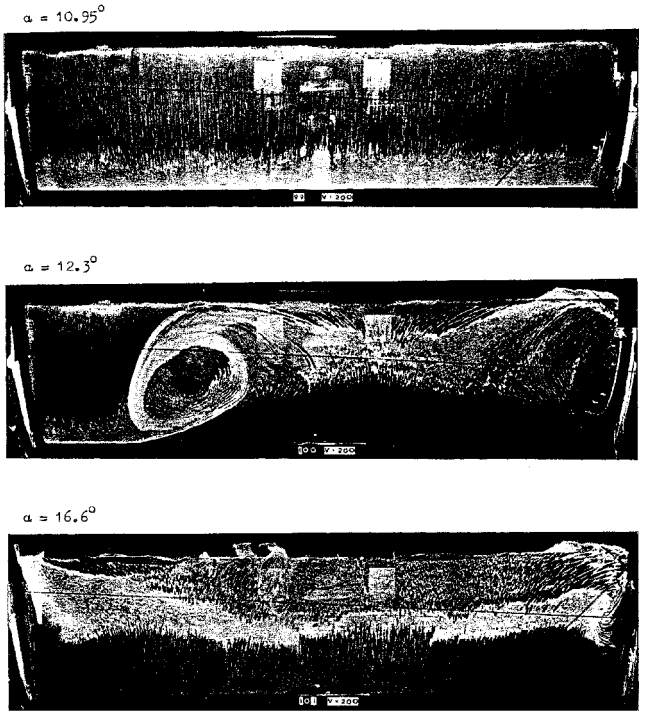

a) Transition fixed, $Re = 1.68 \times 10^6$

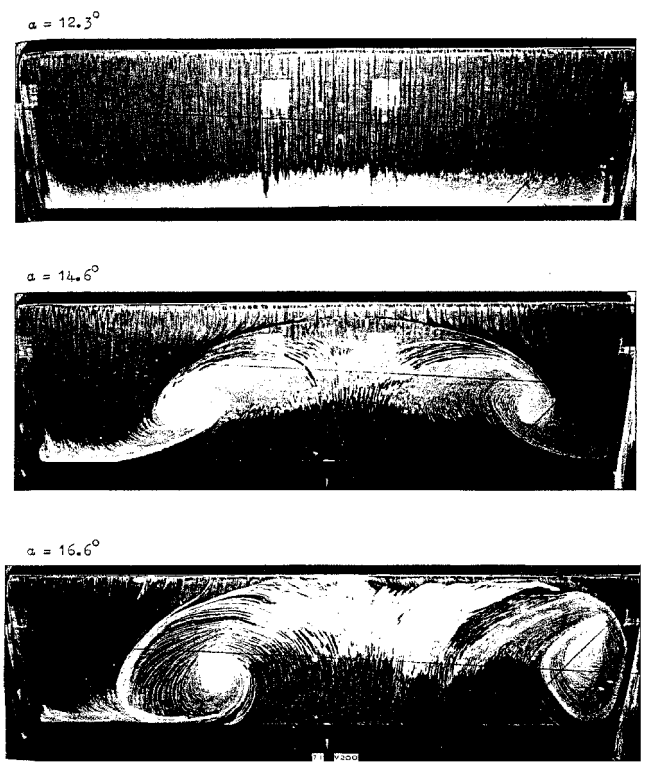

b) Transition free, $Re = 0.84 \times 10^6$

Fig. 3 Upper-surface flow visualization on two-dimensional wing model.[3]

C–D in Fig. 1b produced roughly the same lift as the downstroke branch B–C. This requires the introduction of the "spilled" vortex phenomenon.[9–11]

In the case of the leading-edge stall on the NACA-0012 airfoil, the travel down the chord of the spilled leading-edge vortex[9] (Fig. 7a) is generating lift after that leading-edge stall has occurred. The $C_L(\alpha)$ characteristics[10] in Fig. 7b show that more than one leading-edge vortex is spilled, probably generated by an oscillating separation point,[11] similar to what has been observed for shock-induced flow

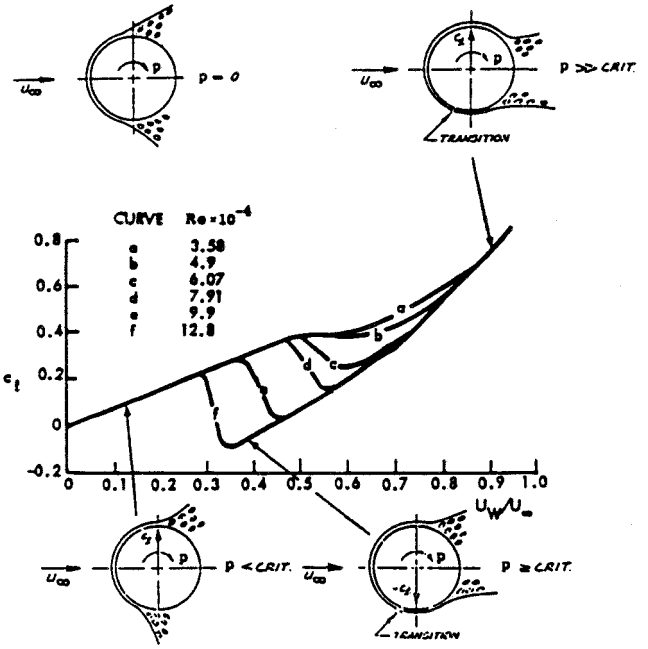

a) At initially laminar flow conditions

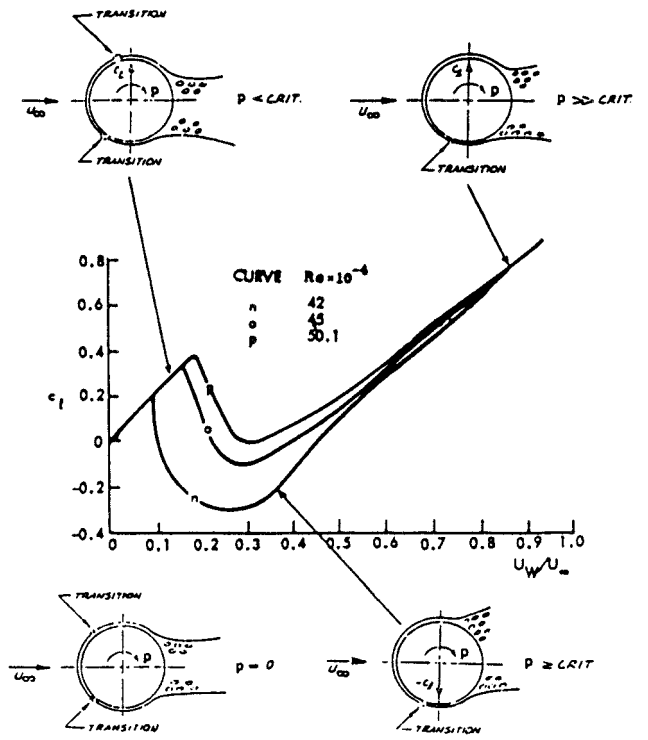

b) At initially turbulent flow conditions

Fig. 4 Magnus lift characteristics of a rotating circular cylinder.[7]

separation[12,13] (Fig. 8). In both cases, the separation point is describing a pseudoharmonic oscillation around a quasi-steady mean position. In the case of low-speed stall (Fig. 7), the separation point progresses almost all the way to the leading edge in the first half-cycle before a leading-edge vortex is shed. In subsequent cycles, the separation point progresses less and less far forward, generating gradually more diminutive vortices. Such a vortex-shedding phenomenon could have maintained the observed high lift level during the upstroke branch C–D in Fig. 1b. Of course, Karman vortex shedding could also establish an oscillating separation point[14] at the reduced frequency $\bar{\omega}_K = 2\pi Sr_K \sin \alpha_o$. For Strouhal frequency $Sr_K = 0.2$ and $\alpha_o \approx 14$ deg, one obtains $\bar{\omega}_K \approx 0.31$, which should be compared to $\bar{\omega} = \omega c / U_\infty = 0.369$ for the airfoil oscillation in Fig. 1b.

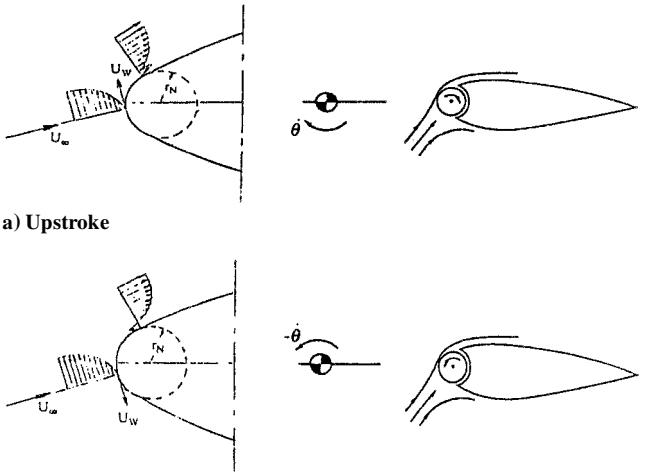

Fig. 5 Moving-wall effect on a pitching airfoil.[6]

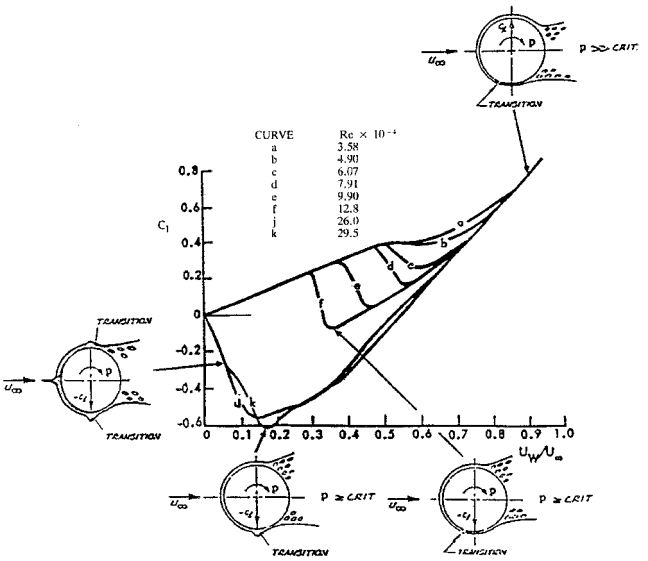

Fig. 6 Effect of boundary-layer transition on the Magnus lift characteristics of a rotating circular cylinder.[7]

Influence of Karman Vortex Shedding

Measurements of the lateral response of a circular cylinder to Karman vortex shedding[15] (Fig. 9) show that the maximum oscillation amplitude occurred at a velocity where the cylinder oscillated at roughly 85% of the Karman shedding frequency. It has been shown[16] that at this frequency the moving-wall effect generated by the Karman vortex shedding can drive the cylinder oscillation most effectively. The oscillation frequency $\bar{\omega} = 0.369$ in Fig. 1b is 18% higher than the Karman shedding frequency $\bar{\omega}_K = 0.31$, corresponding to $f = 1.18\ f_o$ in Fig. 9, demonstrating that there could not be any interaction with the Karman vortex shedding. At $\alpha_o \approx 14$ deg, the airfoil oscillates in and out of stall, and the associated moving-wall effect, discussed earlier, is dominating. Thus, the spilled vortex phenomenon is the flow mechanism most likely to be responsible for modifying the straightforward moving-wall effect to generate the loop variations seen in Fig. 1b. It is the only likely cause of the nonrepeating backstroke branches of the $c_m(\alpha)$ loops for the Vertol 23010-1.58 airfoil,[17] pitching at $\bar{\omega} = 1.4$ (Fig. 10). However, the two different $C_L(\alpha)$ loops in Fig. 1a cannot be explained by the spilled vortex phenomenon. One must, therefore, take another look at a possible interaction between the Karman vortex shedding and the dynamic stall process in the α range 10.95 deg $\leq \alpha \leq$ 11.8 deg. For $\alpha \approx$ 11 deg and $Sr_K \approx 0.2$, one obtains $\bar{\omega}_K = 2\pi Sr_K \sin\alpha \approx 0.236$.

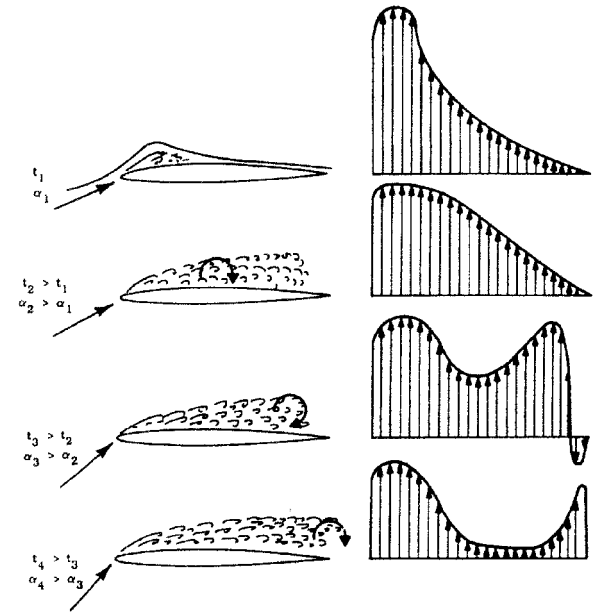

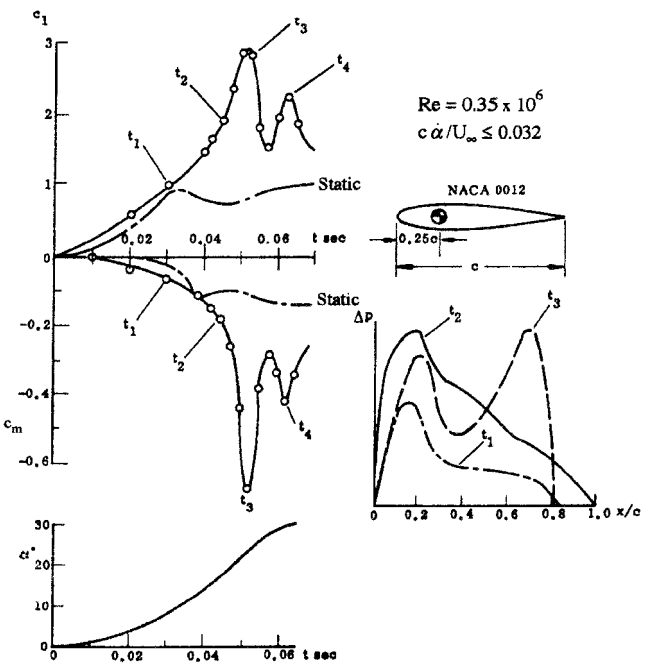

Fig. 7 Spilled vortex characteristics on a pitching NACA-0012 airfoil.

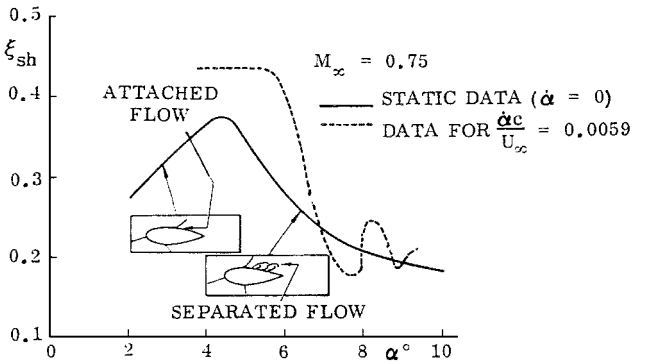

Fig. 8 Pitch-rate-induced oscillation of shock-induced flow separation at $M = 0.75$ (Ref. 13).

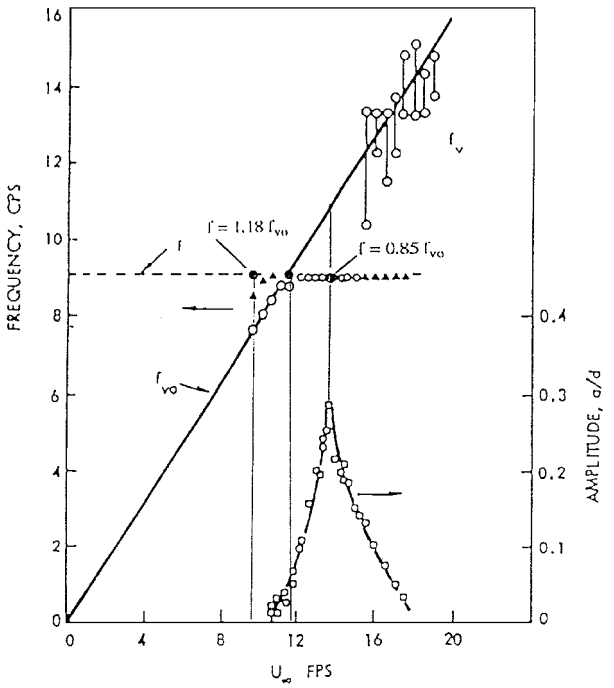

Fig. 9 Coupling between lateral oscillation and Karman vortex shedding.[15]

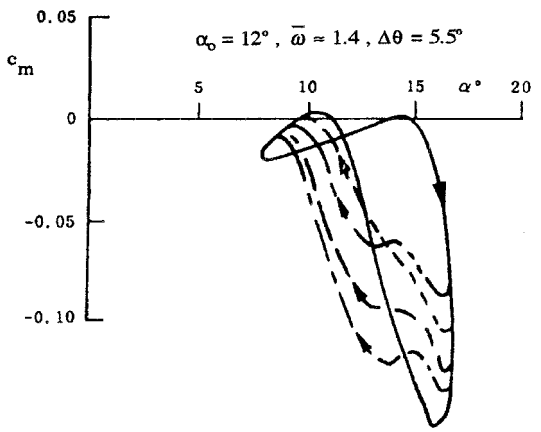

Fig. 10 Nonrepeating backstroke branches of $c_m(\alpha)$ for an airfoil oscillating in pitch.[17]

That is, $\bar{\omega}_K \approx 2\bar{\omega} = 0.234$, and Karman vortex shedding could definitely have caused flow reattachment, subsequently allowing the regular moving-wall effect (Figs. 4 and 5) to generate the high $c_l(\alpha)$ loop DEFG in Fig. 1a. The full $C_L(\alpha)$ time history[3] (Fig. 11) shows how, as expected[16] for $\bar{\omega} = \bar{\omega}_K/2$, the interaction with the Karman vortex shedding was only possible every other cycle of the airfoil oscillation. The figure also shows that the unstalled conditions could not be reached. The reason for this is not that only every other cycle is affected by the moving-wall effects generated by the lateral oscillation induced by the Karman vortex shedding, but rather that the resonance condition gives only 20% of the maximum possible response[16] ($f = f_{vo}$ in Fig. 9). In the case of "transition free" (Fig. 1b), $\bar{\omega} = 0.369$ and no significant interaction with the Karman vortex shedding at $\bar{\omega}_K = 0.236$ was possible, as $f = 1.58 f_{vo}$ in Fig. 9.

Conclusions

The dynamic tests of a NACA-0012 airfoil model, reported by Moss and Murdin in 1968,[3] produced very unusual dynamic stall characteristics, generated by interactions between the following flow phenomena:

1) the accelerated-flow and moving-wall effects on dynamic airfoil stall,

2) the reversal of these effects when they influence flow separation via their effects on boundary-layer transition, and

3) the interaction between the oscillating flow separation and Karman vortex shedding.

Each of these flow phenomena can have strong effects by itself on the dynamic stall characteristics of wind-turbine and helicopter blades. However, the biggest problem is that they can severely distort the dynamic results obtained in subscale tests. As it is readily possible to avoid this problem if appropriate steps are taken in the planning of the test, it is important that the test engineer is aware of these intricate flow interactions.

References

[1]Madsen, H. A., Bak, C., Fuglsang, P., and Rasmussen, F., "The Phenomenon of Double Stall," *European Windturbine Energy Conference 97*, Paper 1997.

[2]Ericsson, L. E., "Role of Stall Flutter in the Double-Stall Phenomenon of Wind-Turbine Blades," *Journal of Aircraft*, Vol. 37, No. 1, 2000, pp. 104–109.

[3]Moss, G. F., and Murdin, P. M., "Two-Dimensional Low-Speed Tunnel Tests on the NACA 0012 Section Including Measurements Made During Pitching Oscillations at the Stall," CP-1145, Royal Aircraft Establishment, Farnborough, England, U.K., May 1968.

[4]Liiva, J., Davenport, F. J., Grey, L., and Walton, I. C., "Two-Dimensional Tests of Airfoils Oscillating Near Stall," Vols. I and II, USAAVLABS TR

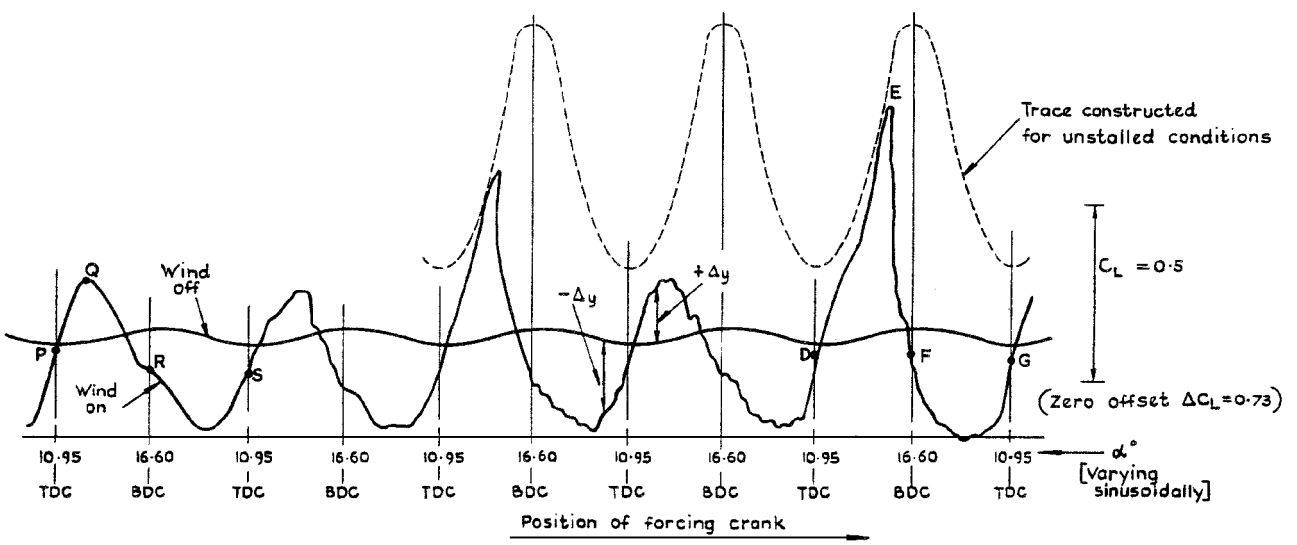

Fig. 11 Multiple-cycle $C_L(\alpha)$ characteristics of NACA-0012 wing model for transition fixed; $Re = 1.68 \times 10^6$, $\alpha_o = 13.78$ deg, $\Delta\theta = 2.83$ deg, and $\bar{\omega} = 0.117$ (Ref. 3).

16–13 A&B, April 1968.

[5]Ericsson, L. E., and Reding, J. P., "Fluid Mechanics of Dynamic Stall, Part I, Unsteady Flow Concepts," *Journal of Fluids and Structures*, Vol. 2, Jan. 1988, pp. 1–33.

[6]Ericsson, L. E., "Moving Wall Effect in Relation to Other Dynamic Stall Flow Mechanisms," *Journal of Aircraft*, Vol. 31, No. 6, 1994, pp. 1303–1309.

[7]Swanson, W. M., "Magnus Effect: A Summary of Investigations to Date," *Journal of Basic Engineering*, Vol. 83, Sept. 1961, pp. 461–470.

[8]Ericsson, L. E., "Effect of Transition on Wind Tunnel Simulation of Vehicle Dynamics," *Progress in Aerospace Sciences*, Vol. 27, 1990, pp. 121–144.

[9]Ericsson, L. E., and Reding, J. P., "Dynamic Stall of Helicopter Blades," *Journal of the American Helicopter Society*, Vol. 17, No. 2, 1972, pp. 11–19.

[10]Ham, N. D., and Garelick, M. S., "Dynamic Stall Consideration in Helicopter Rotors," *Journal of the American Helicopter Society*, Vol. 13, No. 2, 1968, pp. 44–55.

[11]Ericsson, L. E., and Reding, J. P., "'Spilled' Leading-Edge Vortex Effects on Dynamic Stall Characteristics," *Journal of Aircraft*, Vol. 13, No. 4, 1976, pp. 313–315.

[12]Ericsson, L. E., "Dynamic Effects of Shock-Induced Flow Separation," *Journal of Aircraft*, Vol. 12, No. 2, 1975, pp. 86–92.

[13]Lambourne, N. C., "Some Instabilities Arising from the Interaction Between Shock Waves and Boundary Layers," Aeronautical Research Council, CP-473, England, U.K., Feb. 1958.

[14]Ericsson, L. E., "Effect of Karman Vortex Shedding on Airfoil Stall Flutter," *Journal of Aircraft*, Vol. 24, No. 12, 1987, pp. 841–848.

[15]Parkinson, G. V., and Ferguson, N., "Amplitude and Surface Pressure Measurements for a Circular Cylinder in Vortex-Excited Oscillation at Subcritical Reynolds Numbers," *Meeting on Ground Wind Load Problems in Relation to Launch Vehicles*, Paper 18, NASA Langley Research Center, Hampton, VA, June 1966.

[16]Ericsson, L. E., "Karman Vortex Shedding and the Effect of Body Motion," *AIAA Journal*, Vol. 18, No. 8, 1980, pp. 935–944.

[17]Liiva, J., and Davenport, F. J., "Dynamic Stall of Airfoil Sections for High Speed Rotors," *Proceedings 24th Annual National Forum of the American Helicopter Society*, Paper 206, Washington, DC, May 1968.